Complete Characterization of One QUaD Pixel

For Consideration of Honors on the
Degree of Bachelor of Science

Evan Kirby

20 May 2004

Stanford University
Department of Physics

ABSTRACT

The QUaD project will measure the cosmic microwave background's polarization anisotropy from the South Pole beginning in early 2005. This thesis discusses the optical characterization of a single pixel in both the 100 GHz and 150 GHz spectral bands using the QUaD test bed. It describes the methods and results for measuring the pixel's spectral response, polarization response, spatial response, and the optical efficiency. It also estimates the sensitivity of one pair of polarization-sensitive bolometers for each spectral band.

CONTENTS

ACKNOWLEDGEMENTS

The Stanford Undergraduate Research Office supplied a Major Grant which supported this project. I warmly thank the donors who made the grant possible.

I would also like to thank Professor Sarah Church for her kindness and setting aside time to help me whenever I needed it. Her willingness to accept undergraduates into her lab and to teach them about her projects has exposed me to experimental physics research. I am especially indebted to Jamie Hinderks. He has never failed to answer any of my questions, no matter how annoying or inconvenient. I owe nearly everything I know about laboratory research to him. When I say, "we," in this thesis, I mean, "Jamie and I." Ben Rusholme deserves thanks for helping to draft my URO grant proposal. I appreciate John Kovac from Caltech for taking a lot of time out of his schedule to help Jamie and me measure the return loss of the QUaD horns at JPL. Thanks also to Brad Benson, Keith Thompson, Gary Cahill, Samantha Edgington, Mike Zemcov, and my fellow thesis writers Ali Brizius and Cara Henson.

My friends who do not necessarily study physics also deserve my thanks. My suitemates Graham Brown, Dustin King, Spencer Smith, and John Wrobel deserve praise for putting up with my perpetual absence and coming home late, presumably from the lab. I especially appreciate Alexander Rosas for his inspiration. If he didn't work so hard on his thesis, I wouldn't be so motivated to work on mine. At the same time, I owe him and Casey Goodman lots of stress relief, especially for our tradition of making sure we leave campus every Friday.

My parents deserve much of the credit for this thesis for getting me to where I am today. Both the opportunity and determination that made this thesis possible come from Mom and Dad.

Finally, thank you, Truc, for your understanding when I had to stay in lab, for your natural ability to take my mind off of my thesis, and for genuinely caring about me.

1. PROJECT MOTIVATION

The cosmic microwave background (CMB) has three observable properties which each encode different important cosmological information: blackbody frequency spectrum, spatial brightness anisotropy, and linear polarization anisotropy. Recent satellite projects like COBE and WMAP have mapped the frequency spectrum and the spatial brightness anisotropy of the CMB. The remaining CMB property, polarization, has only recently been detected. It is the most challenging to measure because the polarization signal fluctuates less than a μK.

However, polarization measurements of the CMB potentially offer the most insight into the early universe. The polarization components, called the Stokes parameters Q and U, lend their names to QUaD. If a source has intensity I, and a fraction p is linearly polarized at an angle χ with respect to the detector, then Q and U are[1]

$$Q = pI\cos(2\chi) \tag{1.1}$$
$$U = pI\sin(2\chi) \tag{1.2}$$

The polarization structure on the sphere of the sky is commonly split into two components: the gradient of a scalar field and the curl of a vector field. The gradient is closely associated with temperature anisotropy, but slight differences in dependence on the conditions of the early universe can improve our understanding of cosmological parameters. The curl pattern is more exotic. It is predicted that its magnitude is directly proportional to the energy scale of primordial gravitation waves suggested by inflation. Measurements of the curl allow us to probe the first instants of the universe, when its initial conditions were set. These conditions allowed the universe to develop into what we see today.

1.1 The QUaD instrument

QUaD is a new, purpose-built instrument to map the CMB polarization structure scheduled to begin observing at the DASI site at the South Pole

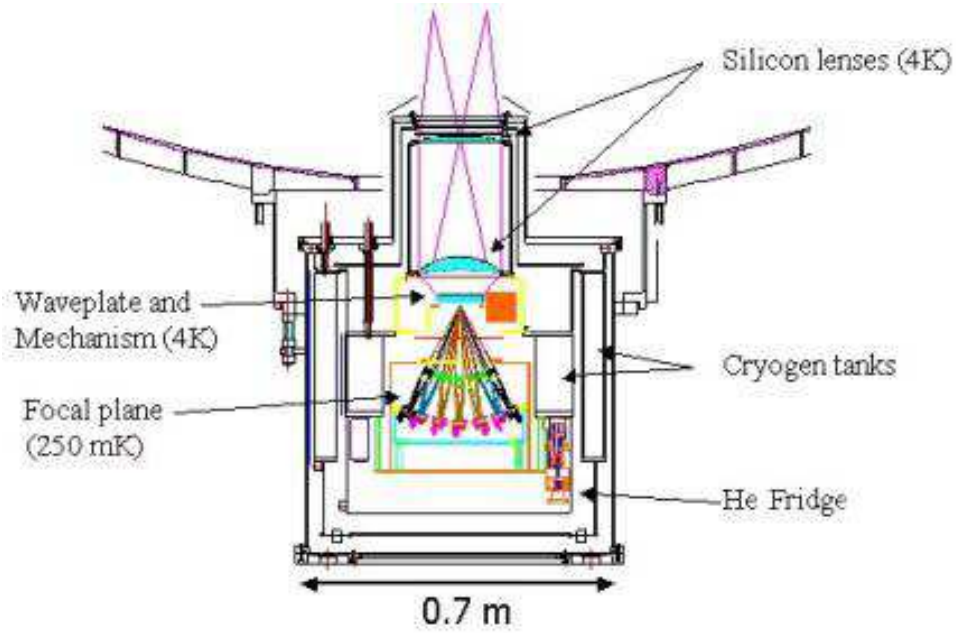

Fig. 1.1: The QUaD receiver on the DASI mount. Ray traces show the path of CMB radiation into the 31 feed horns on the focal plane.

in 2005. (The original project name was QUEST, the Q and U Extragalactic Survey Telescope. Since the Degree Angular Scale Interferometer, DASI, donated its telescope and mount, QUEST has been called QUaD, QUEST at DASI.) Collaborators on the joint project include researchers at Stanford and the University of Wales, Cardiff, with support from Caltech, the National University of Ireland, and the University of Edinburgh. The telescope itself is a 2.64 m Cassegrain dish equipped with a custom receiver designed to measure the polarization in two frequency bands. Stanford's responsibility, under the direction of Professor Sarah Church, is to build this cryogenically cooled receiver array. It will consist of twelve pixels sensitive to CMB radiation in a spectral band around 100 GHz and nineteen pixels in a band around 150 GHz. Figure 1.1 displays a cross section of the QUaD receiver on the DASI mount.

Polarization measurement is QUaD's major contribution to CMB research. The system must preserve incoming polarization very accurately without introducing spurious polarization because either effect will dominate the tiny polarization signal from the sky. The instrument's design minimizes these effects as much as possible. First, the optical system is symmetric to minimize system-induced polarization. Second, the receiver uses perpendicularly oriented polarization-sensitive detectors to sample both axes of linear polarization within the same pixel. Earlier experiments that measured the

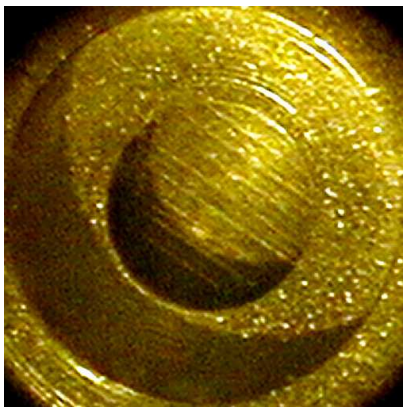

Fig. 1.2: PSB 150-21 magnified 7.5 times. The outer circle accepts the horn mounting flange. The wire mesh is suspended within the inner circle.

two axes of polarization using different pixels had to deal with large offsets in the data. Third, a rotating cryogenic half-waveplate modulates the polarization measured in each pixel. This technique, with the proper implementation, reduces noise by filtering slowly drifting signals such as $1/f$ detector noise.

1.2 Polarization-sensitive bolometers

The devices QUaD uses to measure the CMB polarization are polarization-sensitive bolometers (PSBs). A bolometer is any highly sensitive device which measures radiant heat. Bolometers used in modern microwave experiments consist of a radiation-absorbent substrate in thermal contact with a thermistor. The resistance of the thermistor changes as the incident radiation heats the substrate. The QUaD PSBs are silicon nitride (Si_3N_4) wire meshes.[2] The metallized wires in one axis of the mesh respond to polarized radiation. The unmetallized wires in the orthogonal axis provide structural support and allow radiation to pass through them. Two PSBs mounted orthogonal to each other form the detector for a single pixel. Figure 1.2 shows a PSB that will be used in QUaD.

A bolometer essentially converts an incident optical power to a resistance R_{bolo}. The resistance depends on the bolometer temperature T_{bolo}. A bias current flowing through the bolometer converts R_{bolo} to a measurable voltage V_s. The bias current comes from a voltage source applying a bias voltage V_b, which may be either AC or DC. Two load resistors with resistance R_L comparable to R_{bolo} convert V_b to the bias current I_{bias}.

$$I_{\mathrm{bias}} = \frac{V_b - V_s}{2R_L} \tag{1.3}$$

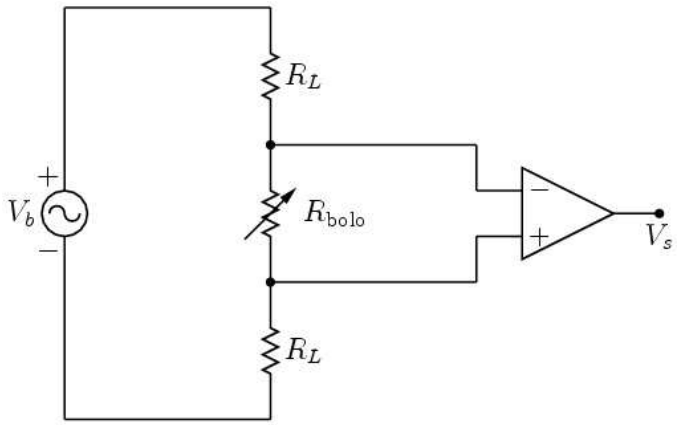

Fig. 1.3: A simplified circuit diagram of the bolometer electronics. The voltage V_b, shown here as AC, biases the bolometer with temperature-dependent resistance R_{bolo} through the load resistors R_L. A differential amplifier measures the voltage across the bolometer, called the signal voltage V_s.

Thus, the simplified circuit (fig. 1.3) is a voltage divider. Ohm's Law gives the bolometer resistance in terms of the measurable signal voltage, the known voltage bias, and the known load resistance.

$$\begin{aligned} R_{\text{bolo}} &= \frac{V_s}{I_{\text{bias}}} \\ &= 2R_L \frac{V_s}{V_b - V_s} \end{aligned} \tag{1.4}$$

The bolometer resistance varies a great deal with temperature, especially at low temperature. Their exceptional sensitivity makes them ideal microwave radiation detectors.

QUaD uses different bolometer modules for the two observing frequencies. Corrugated, profiled electromagnetic feed horns direct the incident microwave radiation into the bolometers. The 100 GHz horns have wider bolometer mounting flanges than the 150 GHz horns. Therefore, only a properly sized bolometer module may mount to the horn. The responses of the two sets of bolometers are nearly identical; they differ only in the size of the horn mount. Each bolometer module obeys a nomenclature convention. An orthogonal pair of PSBs in a 100 GHz mount may be called PSB 100-01, where the last two digits identify each module uniquely. Similarly, an orthogonal pair of PSBs in a 150 GHz mount may be called PSB 150-01. Within a module, the PSB closest to the horn is called "TOP" because QUaD will be an upward-looking dewar. The other PSB is called "BOTTOM." Unfortu-

Fig. 1.4: The test bed focal plane (the gold plate on which the horn rests) in the 100 GHz configuration. The cylinder on the left is the ^{3}He refrigerator, shown here with a aluminum protective immobilizer instead of a copper heat strap to the focal plane. Band-defining filters cap the 100 GHz feed horn at the center of the focal plane. The PSB mounts to the bottom of the horn, under the gold plate. The box to the right of the horn houses the load resistors.

nately, the QUaD test bed is a downward-looking dewar, and in it, the TOP PSB actually resides closer to the ground than the BOTTOM PSB.

1.3 The QUaD test bed

This thesis describes the characterization of a single QUaD pixel in each of the 100 GHz and 150 GHz spectral bands. All experiments described here occur in the QUaD test bed. Although the QUaD receiver houses all thirty-one pixels, the test bed contains only one. Figure 1.4 shows the test bed's focal plane, which contains one pair of PSBs. A helium-3 refrigerator cools to 300 mK the plate containing the apparatus for one entire pixel, which consists of one feed horn for either 100 GHz or 150 GHz microwaves, its

associated low-pass filters, and the pair of PSBs.

Each chapter in this thesis describes one or more parameters that demonstrate QUaD's functionality. Chapter 2 quantifies the pixel's sensitivity to CMB temperature fluctuations. The sensitivity depends on the pixel's spectral response and optical efficiency, both described in the chapter. Chapter 3 describes the pixel's polarization response, including a quantification of how well the system preserves polarization. Chapter 4 presents the method and results for measuring the size and shape of the spatial field to which QUaD is sensitive. Chapter 5 briefly discusses opportunities for continuing research to improve all of the pixel response characteristics. The three appendices serve as supplemental and independent references on microwave bolometers, the sensitivity of CMB bolometer experiments, and Fourier transform spectroscopy.

2. SENSITIVITY ESTIMATE

Given the observing conditions at the South Pole, we expect QUaD to be sensitive to 270 μK $s^{1/2}$ fluctuations in the CMB polarization at 100 GHz and 300 μK $s^{1/2}$ fluctuations at 150 GHz.[3] Photon noise, bolometer noise, and amplifier noise limit the sensitivity. All noise sources added in quadrature yield the total sensitivity of each PSB.

This chapter is devoted to measuring the parameters relevant to calculating the sensitivity of a QUaD PSB. The two relevant parameters for the photon noise are bandwidth $\Delta\nu$ and optical efficiency η. The parameter associated with bolometer noise is the thermal conductance G.

Noise equivalent power (NEP) quantifies noise. The following relations give the photon (shot) and bolometer (phonon) noise:

$$\mathrm{NEP_{phot}}^2 = 2h\nu P_\nu + \frac{2P_\nu^2}{m\Delta\nu} \tag{2.1}$$

$$\mathrm{NEP_{bol}}^2 = 4k_\mathrm{B}T_\mathrm{bolo}^2 G \tag{2.2}$$

where

$$P_\nu = \eta k_\mathrm{B} T_\mathrm{RJ} \Delta\nu \tag{2.3}$$

2.1 Spectral response

QUaD's optical filtering is a delicate balance of maximizing light throughput in the target frequency band while minimizing heat loading. The throat of a corrugated feed horn defines the lower boundary of the band. The corrugations reduce the sidelobes in both the electric and magnetic field planes. Metal mesh filters define the upper edge of the band in addition to blocking stray infrared radiation.

2.1.1 High-pass filtering

The actual QUaD focal plane will contain twelve 100 GHz feed horns and nineteen 150 GHz feed horns. Each horn directs microwave radiation into

Fig. 2.1: A QUaD 100 GHz horn shown with an edge filter, described in section 2.1.2.

Fig. 2.2: A QUaD 150 GHz horn shown with its filter cap.

two orthogonal PSBs. The horns, manufactured by TK Ltd. (UK), are gold-plated copper. The expected cut-on frequency of the 100 GHz horns is 79 GHz, and that of the 150 GHz horns is 128 GHz. Figures 2.1 and 2.2 show both types of horns.

We measure the frequency response of QUaD horns using a vector network analyzer (VNA) because testing each horn individually in the test bed would require 31 separate thermal cycles each lasting approximately one week. Caltech's HP 8720C VNA outputs coherent electromagnetic radiation at a single frequency. As it scans across four hundred frequencies in about an 80 GHz band, it discriminates between the radiation leaving and entering the port. When a feed horn is connected to the port, the "return loss" is any radiation above the horn's cut-on frequency reflected back into the port. The horn does not transmit—in either direction—radiation at frequencies that return to the analyzer. Ideally, the return loss is close to zero, ensuring free, minimally attenuated transmission above the cut-on frequency.

Figure 2.3 shows the return loss for the 100 GHz horn used to gather the data in this thesis. The 79 GHz cut-on is prominent. Most of the 100 GHz horns exhibited anomalously high return loss around 92 GHz. The feature seemed dependent on the horns' mounting to the VNA port and, to a lesser degree, the rotation of the horn. A small gap between the horn and the waveguide adaptors could function as a resonant cavity. The smallest such a resonant cavity could be to produce a 92 GHz feature is half of a wavelength: 1.5 mm. However, the 100 GHz spectral response measured on the FTS also displays a smaller feature around 92 GHz (see fig. 2.9), but the feature shapes and frequencies do not precisely coincide. Therefore, it is unclear that the feature is a property of the feed horn and not its VNA adapters.

Figure 2.4 shows the return loss for the 150 GHz horn #1, the one used to gather the spectral response data in this thesis. The VNA does not have the range to display the 128 GHz cut-on. The optical efficiency, polarization response, and spatial response measurements used horn #2. All of the 150 GHz horns showed very similar return losses with no suspicious features, although we could not probe below 140 GHz. The 150 GHz VNA horn mount differed from the 100 GHz mount, possibly explaining the absence of the 92 GHz feature.

2.1.2 Low-pass filtering

Several metal mesh filters lie in the beam column in order to define the upper band edge. Each filter allows radiation at frequencies lower than its edge frequency to pass through it. However, the filters also leak at the harmonics of their edge frequencies. Therefore, effective band definition requires more than one filter. Even more filters block stray infrared radiation that enter

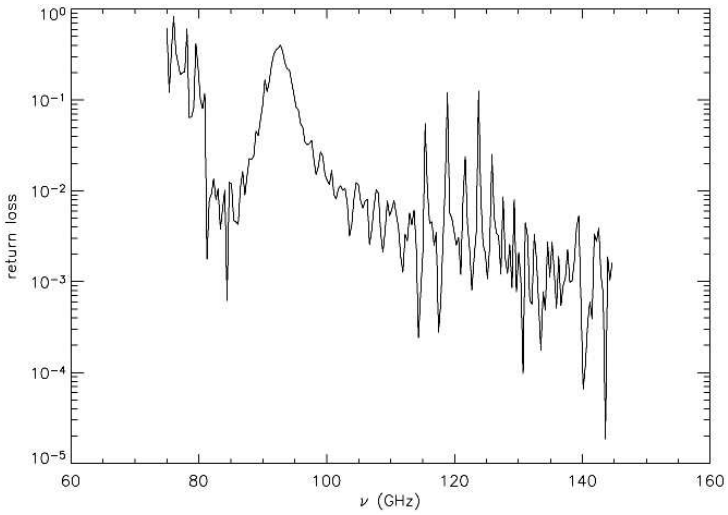

Fig. 2.3: The return loss spectrum for the 100 GHz QUaD horn #9, the one used in all of the 100 GHz testing presented in this thesis. The high return loss at 92 GHz may present a problem for this band.

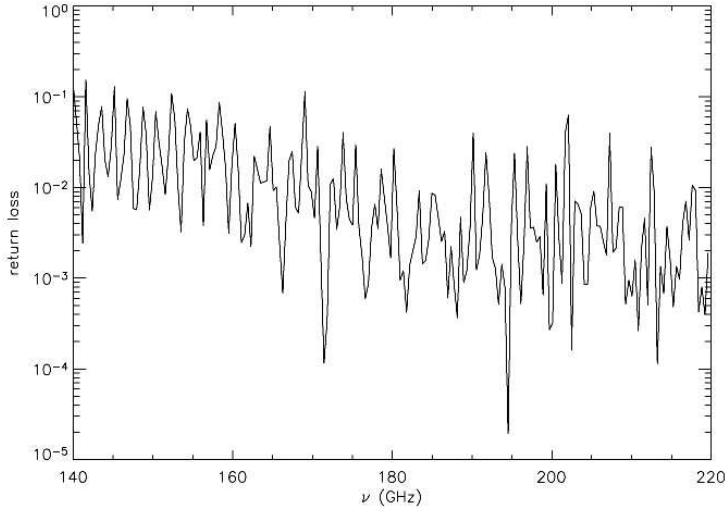

Fig. 2.4: The return loss spectrum for the 150 GHz QUaD horn #1, the one used in the 150 GHz spectral testing presented in this thesis.

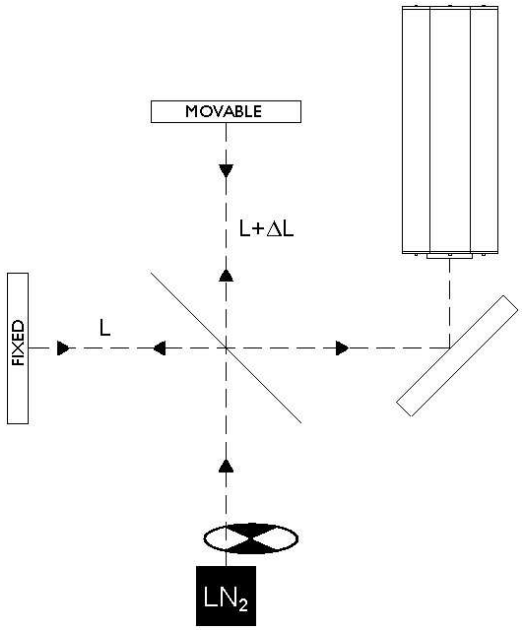

Fig. 2.5: The Fourier transform spectrometer. The liquid nitrogen cold load emits 77 K blackbody radiation which the chopper wheel alternates with 300 K blackbody radiation. The beamsplitter sends the in-phase radiation to both a fixed mirror and a movable mirror. The re-combined, interfering radiation reflects into the QUaD test bed.

and warm the cryostat. Each filter must be placed strategically because the absorbed radiation warms the filter and hence the stage on which it lies. In general, low-pass filters with lower cut-off frequencies should be placed on warmer stages because they reflect more radiation. The filter which passes radiation through the liquid nitrogen thermal shield reflects most of the infrared radiation before it passes through the filters on the liquid helium thermal shield. Filters are identified by their wave number k, given in cm^{-1}. To convert to frequency, multiply k by the speed of light. In units appropriate to microwave astronomy,

$$\nu\ (\mathrm{GHz}) \ = \ 30 \ \times \ k\ (\mathrm{cm}^{-1}) \tag{2.4}$$

This definition, common in infrared astronomy, differs by 2π from some other definitions of wave number.

The most exact method of measuring the full spectral response of the QUaD instrument is Fourier transform spectroscopy. Figure 2.5 depicts a Fourier transform spectrometer (FTS). The device is essentially a Michelson interferometer. A beamsplitter sends incoming radiation from a 77 K liquid nitrogen load optically chopped with 300 K Eccosorb (a rigid foam absorptive

horn	LHe shield	LN_2 shield
3.5 cm^{-1} edge	8 cm^{-1} IR filter	9 cm^{-1} IR filter
3.6 cm^{-1} blocking	12 cm^{-1} IR filter	

Tab. 2.1: Filter configuration for the 100 GHz FTS measurements.

horn	LHe shield	LN_2 shield
5.7 cm^{-1} edge	8 cm^{-1} IR filter	9 cm^{-1} IR filter
6.1 cm^{-1} blocking	12 cm^{-1} IR filter	
5.9 cm^{-1} blocking		

Tab. 2.2: Filter configuration for the 150 GHz FTS measurement.

to microwaves) to a fixed mirror at a distance L and to a movable mirror at a distance $L + \Delta L$. The optical path length difference is $x \equiv 2\Delta L$. The two beams recombine and interfere. Two other mirrors (shown here schematically as one mirror) deflect the interfering radiation into the window of the QUaD test bed. A lockin amplifier measures the bolometer signal voltage, locking on to the frequency of the chopper wheel. A set of measurements at a range of optical path length differences is called an interferogram, and it is the inverse cosine Fourier transformation of the pixel's transmission function.

Tables 2.1 and 2.2 give the filtering configuration for the FTS measurements for each of QUaD's two spectral bands. The IR filters are identical in the two configurations because QUaD will use the same IR filters for all of its horns. Figure 2.6 displays the interferogram for the 100 GHz FTS measurement, and fig. 2.7 displays the 150 GHz interferogram. A mirror misalignment caused the linear drift in the 150 GHz interferogram as the mirror moved away from zero path length difference. The drift does not affect the Fourier transformation because it represents a very low frequency in Fourier space. Regardless, the FTS was re-aligned before the 100 GHz FTS measurement, which displays a reduced linear drift.

Figure 2.8 shows the Fourier transformations of the two interferograms. The maximum transmission is normalized to 1. These curves are the transmission functions of each of QUaD's spectral bands. We define the cut-on and cut-off frequencies to be the frequencies at which the transmission drops to half of the maximum. Table 2.3 summarizes the measured frequency parameters for each type of horn.

The 92 GHz feature that appears in the return loss in fig. 2.3 may also appear in the 100 GHz transmission function in fig. 2.8 as measured on the FTS. Figure 2.9 shows a linear plot of both the return loss and the transmission function for the 100 GHz band. If the 92 GHz ($k = 3.1$ cm^{-1}) feature is an actual effect, a low transmission would accompany a high return

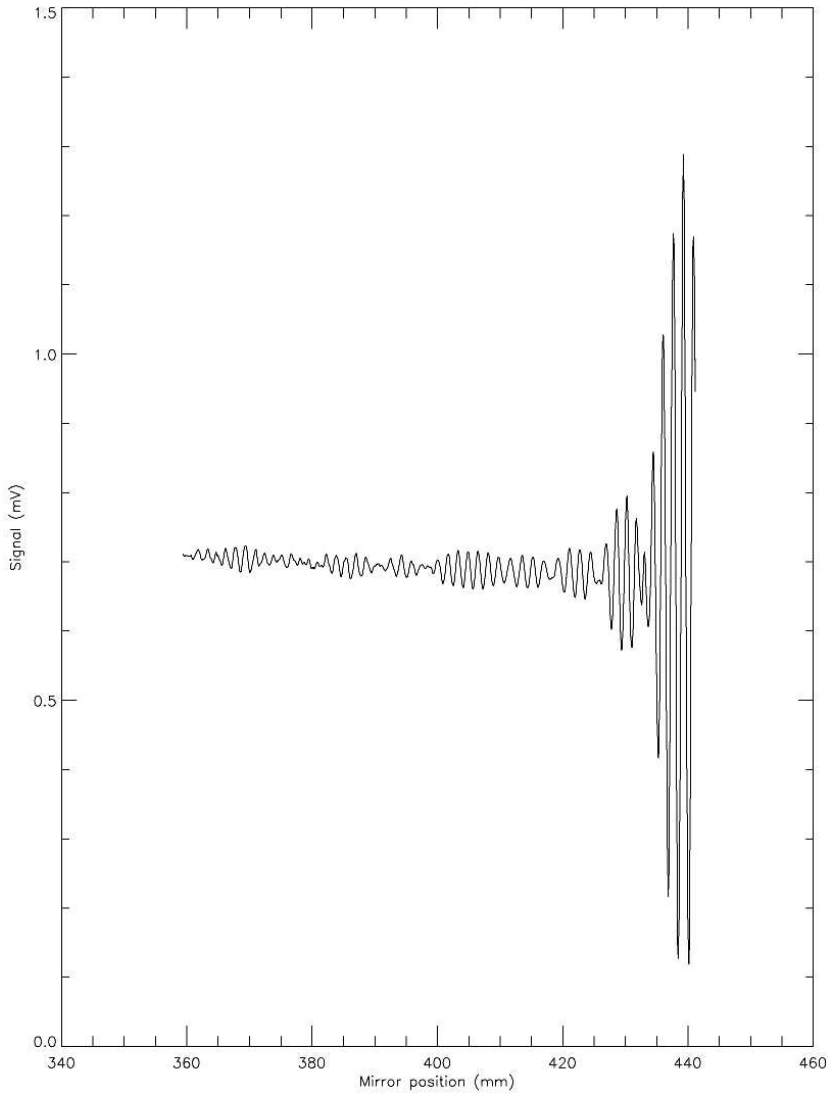

Fig. 2.6: The interferogram from the 100 GHz FTS measurement with PSB 100-14 TOP.

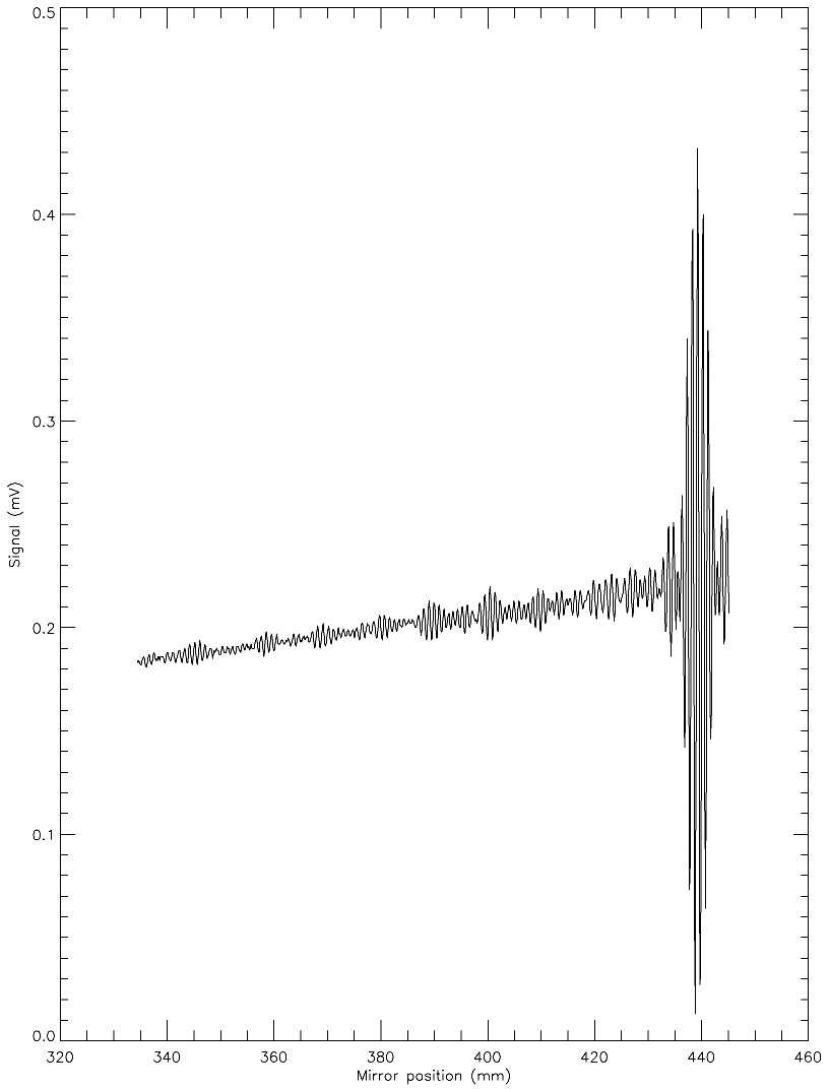

Fig. 2.7: The interferogram from the 150 GHz FTS measurement with PSB 150-02 TOP. A mirror misalignment caused the large linear drift.

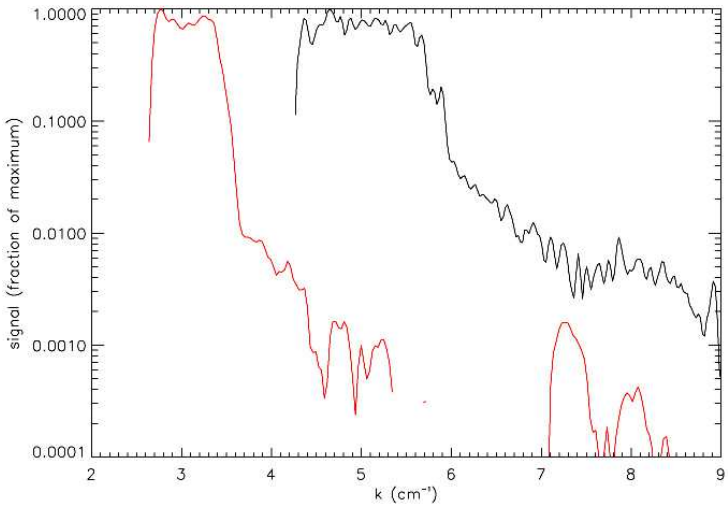

Fig. 2.8: The Fourier transformations of the interferograms from both 100 GHz and 150 GHz configurations. The red line is the Fourier transformation of fig. 2.6 and the black line is the Fourier transformation of fig. 2.7.

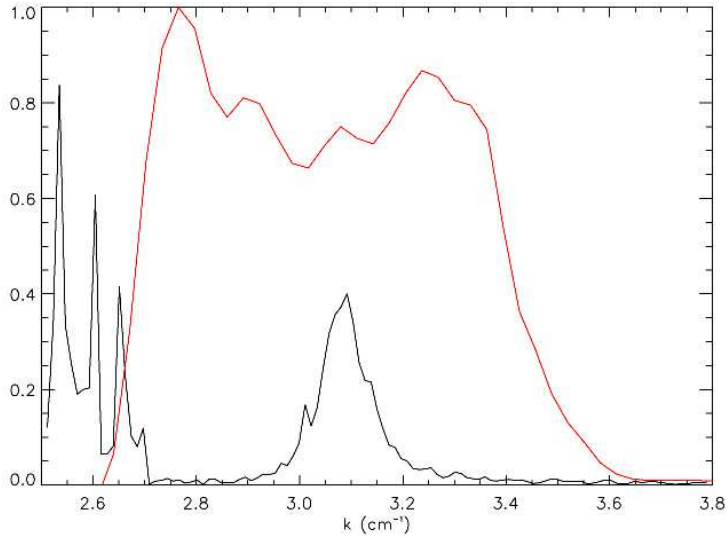

Fig. 2.9: A linear plot of the 100 GHz horn #9's return loss from fig. 2.3 and the transmission function (red) as measured on the FTS from fig. 2.8.

horn	ν_{on}	ν_{off}	$\Delta\nu$	ν_c	fractional bandwidth
100 #9	81	102	21	91.5	0.23
150 #1	132	171	39	151.5	0.26

Tab. 2.3: The cut-on and cut-off frequencies, the bandwidth, the center frequency, and the fractional bandwidth ($\Delta\nu/\nu_c$) for each type of QUaD horn. All frequencies are in GHz.

loss. It is difficult to determine whether the transmission and return loss are correlated. The analysis would benefit from an FTS measurement at higher resolution.

2.1.3 Thick grill filters

The most precise method of determining the existence of an above-band leak is thick grill filtering. A metal plate with many waveguides drilled through it comprises a thick grill filter. The size of the holes determines the very sharp cut-off frequency. Smaller holes yield a higher cut-off frequency. A thick grill filter with a cut-off higher than the band should reduce the signal to nothing if the filters do not leak above their bands.

The QUaD test bed looks at a chopped liquid nitrogen load through

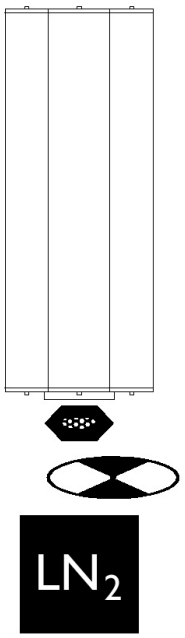

Fig. 2.10: The thick grill filter measurement. The dewar looks at a liquid nitrogen cold load through a filter of small waveguides.

horn	LHe shield	LN_2 shield
5.7 cm^{-1} edge 5.9 cm^{-1} blocking	12 cm^{-1} IR filter	9 cm^{-1} IR filter

Tab. 2.4: 150 GHz filter configuration for thick grill measurement.

a thick grill filter to quantify an above-band leak. First, a lockin amplifier measures the signal without the thick grill filter. Then, it measures the signal with the thick grill filter in place. Figure 2.10 shows a schematic drawing of the experiment. The percentage of the unfiltered signal that passes through the thick grill filter is the percentage of total power reaching the bolometers which is above the cut-off frequency of the thick grill filter. It is important that any structure that holds the filter in front of the window also rests in front of the window during the filterless measurement so that the optical power comparison is accurate. Also, the filter itself attenuates the optical power by a factor that depends on the geometry of the filter. The metal which forms the holes fills roughly half the area of the filter. Therefore, we estimate the filter efficiency to be very approximately 0.5.

A thick grill filter with a 6.38 cm^{-1} cut-off reduced the lockin signal from 2.8 mV to 20 μV with about 3 μV of noise as PSB 100-14 TOP looked at a chopped liquid nitrogen source. The signal disappeared with a 10.20 cm^{-1} cut-off thick grill filter. Therefore, the filter configuration in table 2.1 has a 2×20 μV/2.8 mV = 1.4% power leak between 191 GHz and 306 GHz. The out-of-band leak threatens polarization purity because high frequencies may excite higher order modes in the feed horn. The leak will likely disappear with a different filter configuration.

The 6.38 cm^{-1} thick grill filter reduced the lockin signal from 0.47 mV to less than 0.5 μV as PSB 150-02 TOP looked at a chopped liquid nitrogen source. Therefore, QUaD in the 150 GHz configuration has no out-of-band leaks above 191 GHz to better than 0.2% accuracy. It should be noted that the filter configuration changed between the thick grill measurement and the FTS measurement (see table 2.4). However, the filtering for the FTS measurement used all of the same filters plus two additional ones. Therefore, we assume that the thick grill quantification of the above-band leak remains valid for the FTS configuration.

2.2 Optical efficiency

Optical efficiency quantifies the instrument's receptivity to photons. It represents what fraction of single-polarization radiation in the instrument's spectral band a single PSB oriented in the same polarization axis detects. The

only value required to measure optical efficiency is the difference in optical power at the detector from two sources at different temperatures. This power difference is $Q_2 - Q_1$.

One of the few available definitions of optical efficiency is[4]

$$\eta_{f(\nu)} = \frac{Q_2 - Q_1}{\int_0^\infty A(\nu)\,\Omega(\nu)\,f(\nu)\,\frac{1}{2}[B(\nu,T_2) - B(\nu,T_1)]\,d\nu} \tag{2.5}$$

$A\Omega = \lambda^2$ in a diffraction-limited system such as QUaD. The factor of 1/2 in the denominator comes from the rejection of one polarization, or half of the light of an unpolarized source. The equation simplifies in the Rayleigh-Jeans limit, which is valid for our sources: $T_1 = 77$ K and $T_2 = 300$ K.

$$\eta_{f(\nu)} = \frac{Q_2 - Q_1}{k_\mathrm{B}(T_2 - T_1)\int_0^\infty f(\nu)\,d\nu} \tag{2.6}$$

Despite the mathematical definition, the meaning of optical efficiency remains ambiguous. The confusion enters from the ambiguity in the instrument's "spectral band." Optical efficiency may also be defined as the detected percentage of photons in the entire band passing through the window. In that case, the transmission function becomes a top hat over the bandwidth.

$$\eta_{\Delta\nu} = \frac{Q_2 - Q_1}{k_\mathrm{B}(T_2 - T_1)\Delta\nu} \tag{2.7}$$

On the other hand, FTS measurements give the precise spectral transmission. The transmission function $f(\nu)$ is difficult to normalize because bolometers are not designed to measure an absolute power. Hence, the differential optical efficiency measurement provides the normalization. If $f(\nu)$ is normalized such that its maximum value is 1, then the optical efficiency $\eta_{f(\nu)}$ is defined to be the actual transmission of the maximum value.

Page 41 provides the procedure for measuring a differential optical power. A load curve is taken for each PSB as the dewar looks at 77 K liquid nitrogen, and another is taken as the dewar looks at 300 K Eccosorb. The sources must fill the beam (see Chapter 4) so that they alone optically load the PSBs. Figure 2.11 depicts the dewar looking at each source in succession.

Figures 2.12 and 2.13 show the load curves for each bolometer in the PSB 100-14 module, and figs. 2.14 and 2.15 show the load curves for the PSB 150-21 module. In the graphs on the left, the bias and signal voltages have been converted to bolometer resistance and electrical power dissipated in the bolometer following the prescription in Appendix B. The curves at lower electrical power P correspond to a higher optical power Q according to eq. (B.10). The difference in electrical power $\Delta P = P_1 - P_2$ is equivalent

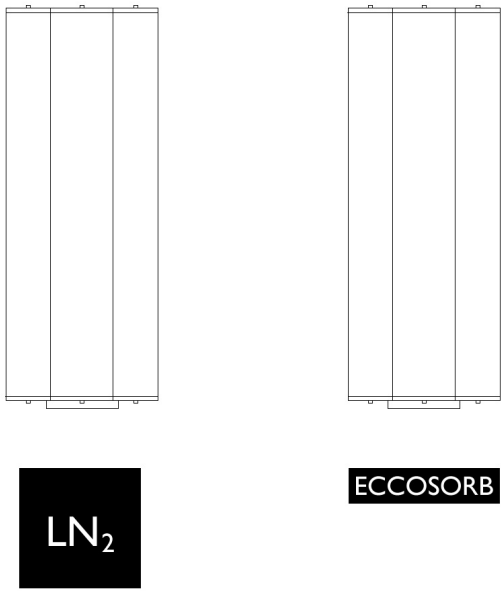

Fig. 2.11: The optical efficiency measurement. First, the dewar looks directly at a liquid nitrogen cold load. Then, it looks directly at 300 K Eccosorb. In each configuration, the signal is recorded for the full range of voltage bias on the bolometer.

to the difference in optical power $Q_2 - Q_1$ along the lines of constant R_{bolo}, shown in the graphs on the right. This difference should be constant for all values of R_{bolo}, but the curves are very close to each other for small R_{bolo}. Therefore, we assume the actual $Q_2 - Q_1$ corresponds to the higher R_{bolo} values, which are still small enough for the E-field effect (see page 39) to remain negligible.

It is important that the base temperature remain constant throughout the load curve. Therefore, a PID (principal, integral, derivative) temperature controller powered a heater on the focal plane during the load curves for

PSB	$Q_2 - Q_1$	$\eta_{f(\nu)}$	$\eta_{\Delta\nu}$
100-14 TOP	21.0 pW	0.624	0.345
100-14 BOTTOM	19.1 pW	0.568	0.314
150-21 TOP	46.7 pW	0.477*	0.394*
150-21 BOTTOM	43.2 pW	0.441*	0.364*

* PSB 150-02 provides the spectral parameters used to determine these optical efficiencies.

Tab. 2.5: Measured optical power differences and optical efficiencies for two PSB pairs. $\eta_{f(\nu)}$ represents the optical efficiency definition of eq. (2.6) and $\eta_{\Delta\nu}$ represents that of eq. (2.7).

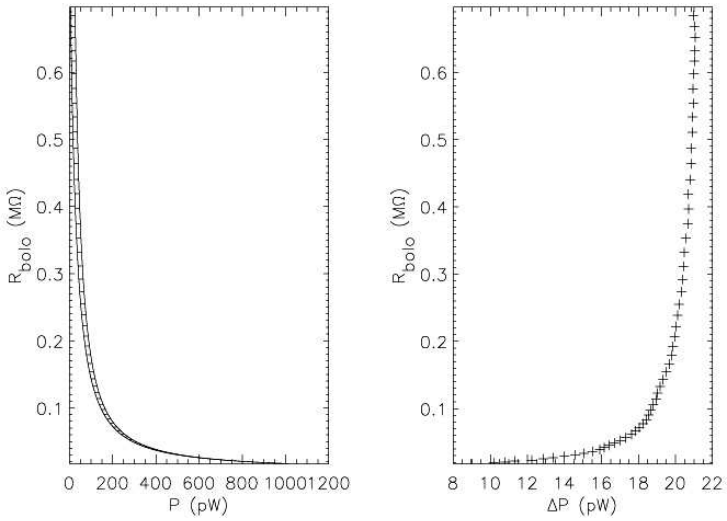

Fig. 2.12: The load curves for PSB 100-14 TOP, for which $T_{\text{base}} = 332$ mK with temperature controlling. The voltages have been converted to bolometer resistance and electrical power. The graph on the left shows the load curves with lines of constant R_{bolo}. The smaller P for each R_{bolo} corresponds to the 300 K load curve, which produces the larger optical loading Q. The greater P for each R_{bolo} corresponds to the 77 K load curve. The graph on the right shows the difference in electrical power for each line of constant R_{bolo}.

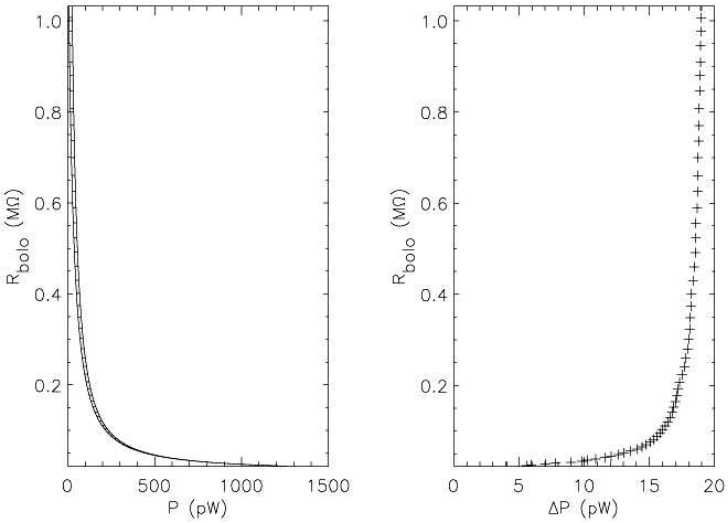

Fig. 2.13: The load curves for PSB 100-14 BOTTOM, for which $T_{\text{base}} = 332$ mK with temperature controlling.

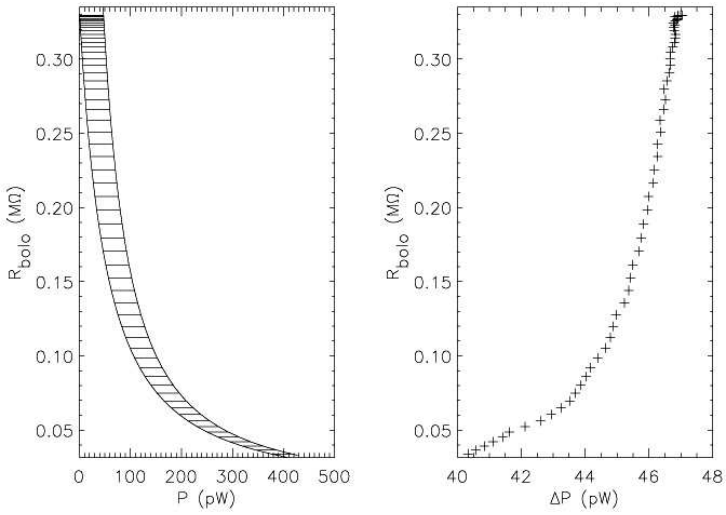

Fig. 2.14: The load curves for PSB 150-21 TOP, for which $T_{\mathrm{base}} \approx 321$ mK without temperature controlling.

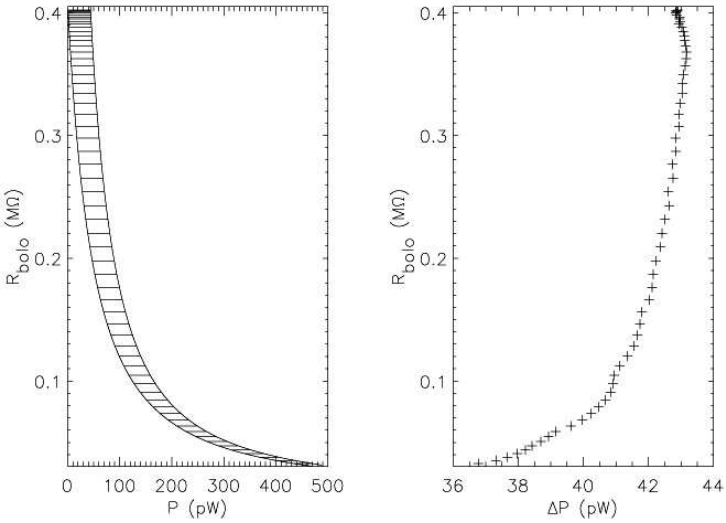

Fig. 2.15: The load curves for PSB 150-21 BOTTOM, for which $T_{\mathrm{base}} \approx 321$ mK without temperature controlling.

PSB 100-14. The temperature remained steadily at 332 mK. Although we did not control the temperature of the focal plane for the PSB 150-21 load curves, it remained within a few mK of 321 mK.

With $Q_2 - Q_1$, eq. (2.5), (2.6), or (2.7) gives the optical efficiency of the single PSB. Table 2.5 gives the optical power differences (from figs. 2.14 and 2.15) and optical efficiencies for each of the two PSB pairs used for most of this thesis.

2.3 Sensitivity estimate

Equation (2.1) gives $\mathrm{NEP_{phot}}$ for the measured values of $\eta_{\Delta\nu}$ and $\Delta\nu$. $\eta_{\Delta\nu}$ must be used because eq. (2.3) uses the bandwidth instead of an integral over the transmission function. Equation (2.2) gives $\mathrm{NEP_{bol}}$ using previously measured thermal conductances for the bolometers. The amplifier noise is assumed to be $\mathrm{NEP_{amp}} = 3.6{\times}10^{-17}$ W $\mathrm{Hz}^{-1/2}$ for every bolometer. Table 2.6 gives all of the NEPs and the NET for PSBs 100-14 and 150-21.

	100-14 T	100-14 B	150-21 T	150-21 B
G(340 mK) (pW/K)	160*	160*	177	202
$\mathrm{NEP_{bol}}$ (10^{-17} W $\mathrm{Hz}^{-1/2}$)	3.2*	3.2*	3.4	3.6
$\mathrm{NEP_{phot}}$ (10^{-17} W $\mathrm{Hz}^{-1/2}$)	2.9	2.7	4.8	4.6
$\mathrm{NEP_{amp}}$ (10^{-17} W $\mathrm{Hz}^{-1/2}$)	3.6	3.6	3.6	3.6
$\mathrm{NEP_{tot}}$ (10^{-17} W $\mathrm{Hz}^{-1/2}$)	5.6	5.5	6.9	6.8
NET (μK $\mathrm{s}^{1/2}$)	350	370	290	310

* G for PSB 100-14 is not available. These numbers come from another 100 GHz bolometer.

Tab. 2.6: A summary of thermal conductances G, NEP components, and the total NET for four PSBs. "T" and "B" stand for "TOP" and "BOTTOM."

3. POLARIZATION RESPONSE

QUaD's purpose is to measure the polarization of the CMB. Therefore, it must independently measure both linear polarizations. The system must preserve the polarization on the sky without introducing spurious polarized signals. Cross-polarization (XP) is the rotation into both polarization axes of a completely polarized signal. The most common sources of XP are a finite polarized response from the bolometer's unmetallized structural wires and higher order mode propagation in the feed horn. The polarization of waveguide modes above the fundamental is not preserved in the horn. Therefore, the band-defining filters in the horn should truncate the frequency band before the onset of higher order mode excitation. Instrumental polarization (IP) is the polarizing of a completely unpolarized signal. The most common source of IP is reflections within the dewar. Much of the material near the beam column is aluminum, which is completely reflective to microwaves. The most effective ways to eliminate IP are to widen the windows so that beam defined by the feed horn is not truncated and to "blacken" aluminum surfaces near the beam with a microwave-absorbing material such as Eccosorb epoxy.

3.1 Cross-polarization

Measuring the cross-polar response of the system requires a source with a single linear polarization. Figure 3.1 shows a microwave polarizer. Parallel copper wires embedded in a 1.5 μm sheet of Mylar linearly polarize microwave light passing through them. A simple diffraction experiment may accurately measure the wire spacing d. A laser shines through the grating onto a screen, shown in fig. 3.2. Let the distance of the m^{th} order point from the central point be y_m, and let the distance from the polarizer to the screen be x. The laser's wavelength is λ.

$$\begin{aligned} \sin\theta &= \frac{m\lambda}{d} \\ &= \frac{y_m}{\sqrt{x^2 + y_m^2}} \end{aligned} \tag{3.1}$$

This diffraction method gives $d = 9.8$ μm.

Fig. 3.1: The polarizer.

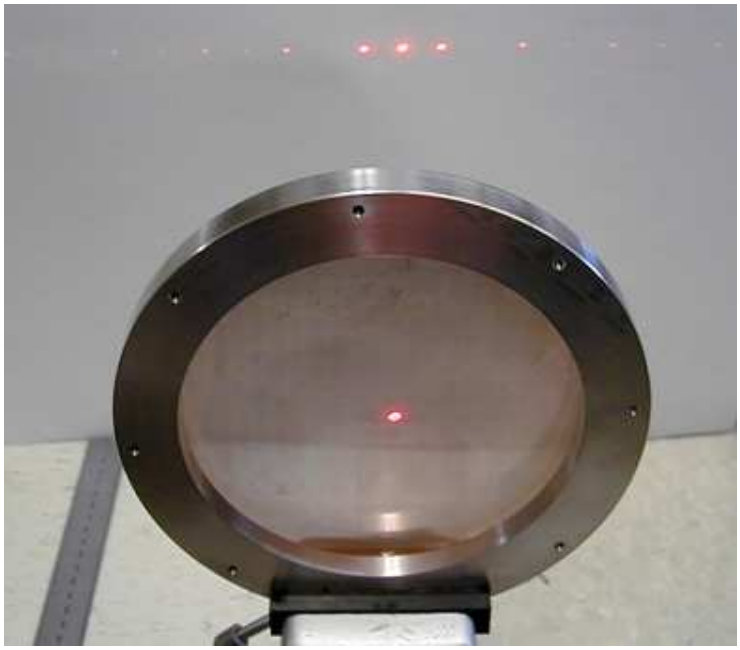

Fig. 3.2: Measuring the polarizer's wire spacing d.

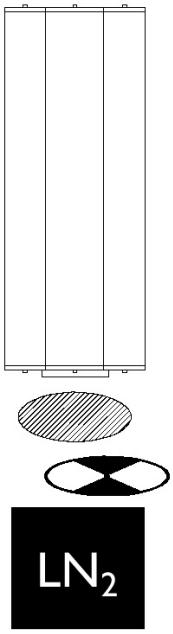

Fig. 3.3: The cross-polarization measurement. The dewar looks at a chopped liquid nitrogen cold load through the polarizer. The polarizer rotates in place, and the bolometer signal is recorded for many angles of rotation.

The polarizer's efficiency may be tested by placing one polarizer directly over an identical polarizer with their polarization axes orthogonal to each other. A single PSB of the QUaD test bed looks through both polarizers at a liquid nitrogen cold load chopped at about 10 Hz. First, we orient the dewar and the polarizer so that the signal is maximal. We call this signal $V_{\max}$. Then, we place another polarizer on top of the existing one and rotate it until the signal from the lock-in amplifier reaches a minimum. We call this signal $V_{\min}$. The ratio $V_{\min}/V_{\max}$ gives the percentage of light of the undesired polarization that passes through the polarizer. We find the grids to be better than 99.96% effective at 150 GHz. Given this high efficiency, we assume the grids to be perfect polarizers.

Measuring the system's XP is a similar process. The QUaD test bed looks at the same chopped liquid nitrogen load through only one polarizer. A computer repeatedly rotates the grid about 8.4° and records the signal from a single PSB through a lock-in amplifier. The resulting graph of the signal versus polarizer rotation should be a sine wave. If the maximum value is normalized to 1, the minimum value is the XP, or the percentage of the completely polarized signal detected in the PSB oriented in the orthogonal direction. Let the sine wave be

$$V = A \ \sin(\theta + \phi) + A_0 \tag{3.2}$$

where V is the signal, A is the amplitude of the wave, A_0 is its offset from zero, θ is the rotation of the polarizer, and ϕ is a phase that depends on the initial position of the polarizer. The normalization requires that $A + A_0 = 1$. The XP is very simply

$$\mathrm{XP} = A - A_0 \tag{3.3}$$

Figure 3.4 shows the cross-polar response of PSB 100-14 TOP. The sine wave fits the data very well even though the error bars (the standard deviation of all of the lockin amplifier samples) on each data point are so small that they are invisible. The line which skims the troughs of the sine wave is the XP, which is 7.50% for this PSB. The above-band frequency leak (see section 2.1.3) may explain the high XP. On the other hand, the XP is only 1.81% for PSB 150-21 BOTTOM, as shown in fig. 3.5.

It was in cross-polarization measurements that we discovered a flaw in the PSB 150-02 module. All XP measurements with those PSBs were higher than 10%. Eventually, we discovered a surprisingly low resistance between the TOP and BOTTOM PSBs, indicating an electrical short. An electrical short often implies a thermal short, as well. Both effects strongly couple the PSBs. Such a PSB will respond to polarized radiation even though it may strike orthogonally to its sensitive axis. The flaw may be limited to polarization response. However, it is possible that it affects both the FTS and thick grill filter measurements presented in section 2.1, both of which used the PSB 150-02 module.

3.2 Instrumental polarization

Each PSB responds differently to the same signal. The lock-in amplifier signal from one PSB looking at an unpolarized liquid nitrogen load may not be the same strength as the orthogonal PSB looking at the same load, even if the IP is near zero. The responses of all the PSBs may be referenced to each other through their load curves. The IP is simply the percentage change in this power difference between the orthogonal PSBs. The optical efficiency measurements (see section 2.2) provide exactly the required data: the difference in measured optical power between a 77 K source and a 300 K source.

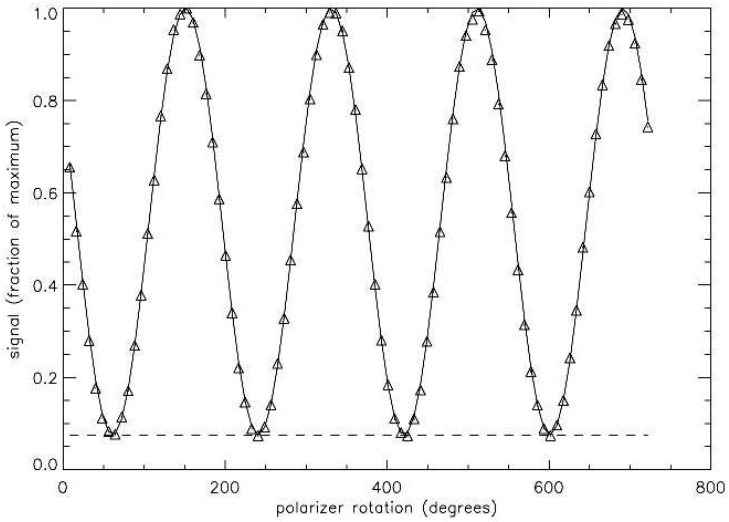

Fig. 3.4: The cross-polarization of PSB 100-14 TOP and its best-fit sine wave. The dashed line is the cross-polar response of this bolometer: 7.50%.

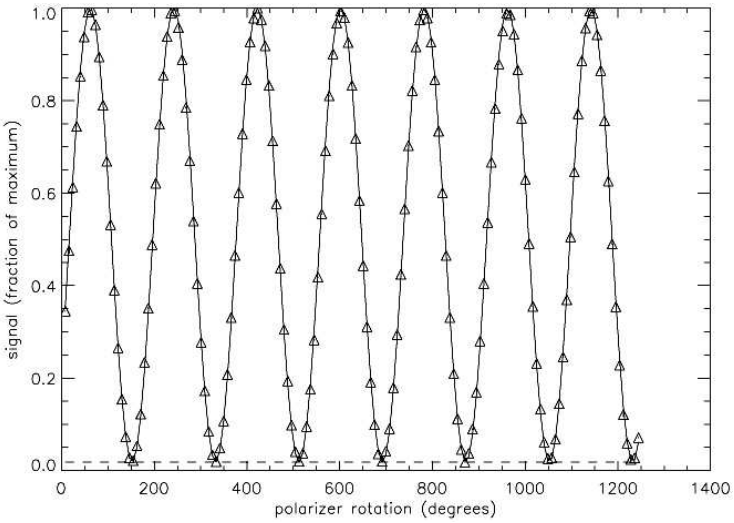

Fig. 3.5: The cross-polarization of PSB 150-21 BOTTOM and its best-fit sine wave. The dashed line is the cross-polar response of this bolometer: 1.81%.

$$\begin{aligned} \mathrm{IP} &= \frac{(Q_2 - Q_1)_\parallel - (Q_2 - Q_1)_\perp}{\max((Q_2 - Q_1)_\parallel,\ (Q_2 - Q_1)_\perp)} \\ &= \frac{\eta_\parallel - \eta_\perp}{\max(\eta_\parallel,\ \eta_\perp)} \end{aligned} \tag{3.4}$$

Optical efficiency and IP measurements are not easily separable. The optical efficiencies cited in section 2.2 incorporate some polarization effects. Similarly, the IP measurement incorporates some optical efficiency effects. The measurements are not independent. However, the dependence is unimportant for data reduction. In order to compare the signal from a TOP bolometer to a BOTTOM bolometer, one simply needs to use the IP as defined in eq. (3.4) as a conversion factor. That relation accounts for both difference in bolometer efficiencies and spurious polarization.

Table 2.5 gives the optical efficiencies relevant to eq. (3.4). In the QUaD test bed, PSB 100-14 has an IP of 9.0%, and PSB 150-21 has an IP of 7.5%.

4. SPATIAL RESPONSE

Accurate spatial response is the third of QUaD's criteria for basic functionality. The CMB polarization maps which QUaD produces will be reliable only if the dewar actually looks at the correct field on the sky. The feed horn defines the size and shape of the beam, but the dewar itself may introduce complications. For example, the filter and window apertures must be wide enough to admit almost all of the power in the beam. Truncating the beam reduces the number of photons reaching the bolometers. Furthermore, reflections inside the dewar may distort the beam significantly. Blackening the aluminum 4 K radiation shield reduces unwanted radiation entering the horn.

QUaD's low-pass filtering cuts off the admitted frequencies before the excitation frequencies for modes of higher order than the fundamental. The electric field of the fundamental mode of a Gaussian beam obeys[5]

$$\psi_0 \propto \frac{1}{\omega} \exp\Big(-\frac{r^2}{\omega^2}\Big) \tag{4.1}$$

where r is the displacement from the axis of the beam and ω is the radius at which the electric field drops by a factor of e. QUaD will always look at thermal, incoherent radiation. Therefore, we are justified in ignoring the phase factors in eq. (4.1). ω is given by

$$\omega^2 = \omega_0^2\Big[1 + \Big(\frac{\lambda z}{\pi\omega_0^2}\Big)^2\Big] \tag{4.2}$$

where z represents the displacement along the axis of the beam from the "phase center," the narrowest point of the beam, for which $\omega = \omega_0$, the beam waist. The beam power within a radius r is proportional to $|\psi_0|^2$.

$$P(r) \propto \frac{1}{\omega^2} \exp\Big(-\frac{2r^2}{\omega^2}\Big) \tag{4.3}$$

The full width at half-maximum of the beam power is $\omega\sqrt{2\,\ln 2} = 1.18\omega$.

Beam mapping is the method of measuring the instrument's spatial response. The dewar rests atop a port on a light-tight box. Eccosorb lines every inside wall of the box. A bucket of liquid nitrogen rests under a hole in the bottom wall. A chopper wheel just under this aperture allows the

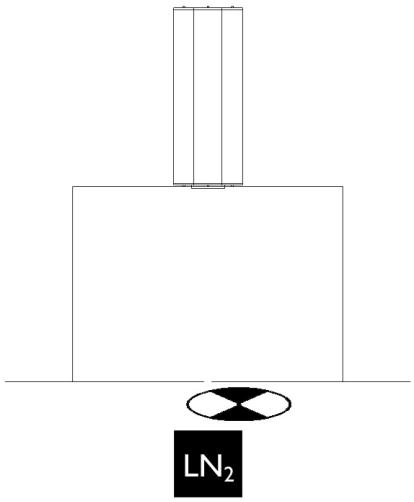

Fig. 4.1: The beam mapper. The aperture, the chopper wheel, and the cold load translate left and right while the dewar remains stationary atop the light-tight, Eccosorb-lined box.

dewar to look alternately at 77 K liquid nitrogen and 300 K Eccosorb. The entire bottom wall of the box, including the chopper wheel and the cold load, translates along one axis. The remaining five walls and the dewar remain stationary. Thus, the source aperture moves in slow, steady increments from one wall to the other, covering the detectable range of the feed horn's optical beam.

Ideally, the same optical power reaches the dewar window regardless of the source position. However, three effects reduce the amount of power that actually reaches the window as the source distance increases. Let θ be the angle of the source with respect to a line drawn perpendicular to the dewar window. First, the source's recession reduces the apparent area of the aperture by $\cos\theta$. Second, the recession increases the distance from the aperture to the window by $\cos^{-1}\theta$. The $1/r^2$ reduction of power reaching the window introduces an additional $\cos^2\theta$ reduction in power. Finally, the bottom wall of the beam mapper box has a finite thickness. As the source recedes, the aperture wall increasingly obscures the source. The attenuation is the ratio of the area which two identical ellipses overlap to the area of one whole ellipse. It depends on θ, the aperture diameter $d = 2.69$ cm, and the aperture thickness $t = 0.55$ cm. If P_0 is the optical power reaching the dewar window when the source aperture lies directly under the dewar, then the power reaching the dewar window as the aperture translates is

$$P = P_0 \cos^3\theta \left(\frac{2}{\pi d^2}\right) \times \left(d^2 \arcsin\left(1 - \frac{t\tan\theta}{d}\right) + (d - t\tan\theta)\sqrt{2dt\tan\theta - (t\tan\theta)^2}\right) \quad (4.4)$$

A feed horn's profile determines ω_0 and the location of the phase center. The metal filter caps which hold the band-defining filters against the mouth of the horn also guide electromagnetic waves. They shift the horn's phase center and, unfortunately, affect the beam shape unpredictably. The end of this chapter describes some of their effects. For QUaD's 100 GHz horns, the beam waist ($\omega_0 = 6.74$ mm) lies 30 mm into the horn from the end of the filter cap. For the 150 GHz horns, the beam waist ($\omega_0 = 4.5$ mm) lies 16 mm from the end of the filter cap. Figures 4.2 and 4.3 depict ω as a function of z. For each type of horn, the dotted lines show the positions of the end of the filter caps, the high density polyethylene dewar window, and the source aperture for the beam mapper.

Given ω at the beam mapper source aperture and the correction in eq. (4.4), we expect the full widths at half-maximum of the Gaussian beams in the plane of the aperture to be 14.2 cm for a 100 GHz horn and 12.4 cm for a 150 GHz horn. Figures 4.4 and 4.5 show measured and expected beam maps for each frequency band. The measured data has not been altered beyond normalization of the maximum to 1. The expected beam maps assume monochromatic beams at the center frequency of each band (from table 2.3), and they are corrected per eq. (4.4). The measured full widths at half-maximum are 13.4 cm at 100 GHz and 11.7 cm at 150 GHz.

Five additional effects serve to alter the width and shape of a beam. First, the beam is not monochromatic. A polychromatic correction incorporates the frequency dependence of ω in eq. (4.3). The correction weights each frequency-dependent Gaussian by the value of the transmission function (fig. 2.8) at that frequency.

$$P(r) \propto \int_0^\infty \frac{f(\nu)}{\omega^2(\nu)} \exp\left(-\frac{2r^2}{\omega^2(\nu)}\right) d\nu \quad (4.5)$$

The polychromatic correction does not alter the beam significantly. A numerical integration with the measured $f(\nu)$ affects the width of the beam map by less than 1%.

The finite size of the beam mapper aperture causes the second effect. The dewar sees an aperture of diameter d, not a point source. We approximate the finite aperture correction by an integral of the Gaussian in eq. (4.3) over the area of the aperture.

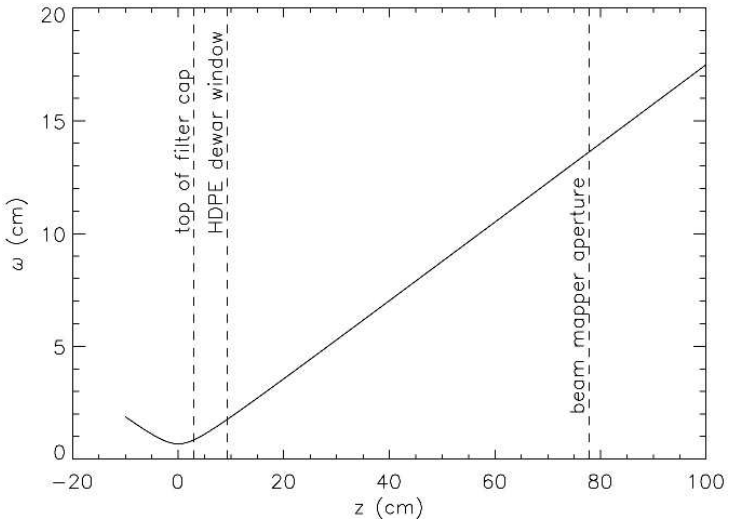

Fig. 4.2: ω as a function of displacement from the phase center along the beam axis for a 100 GHz QUaD horn. The dotted lines show the positions of the end of the horn's filter cap, the dewar window, and the beam mapper source aperture.

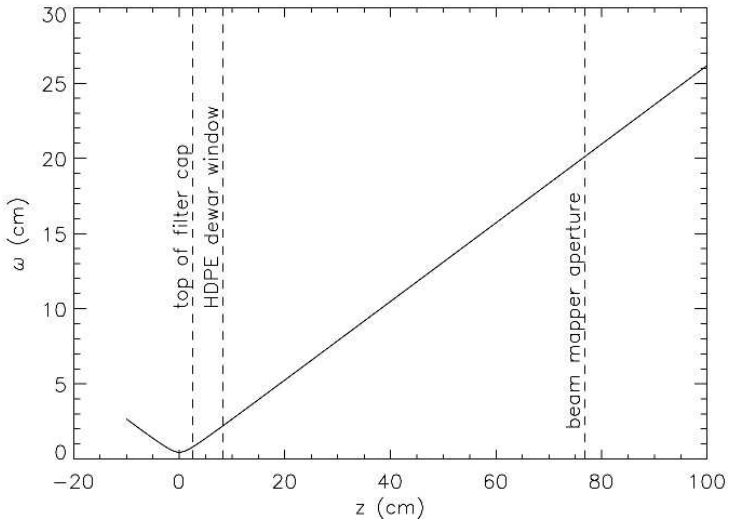

Fig. 4.3: ω as a function of z for a 150 GHz QUaD horn.

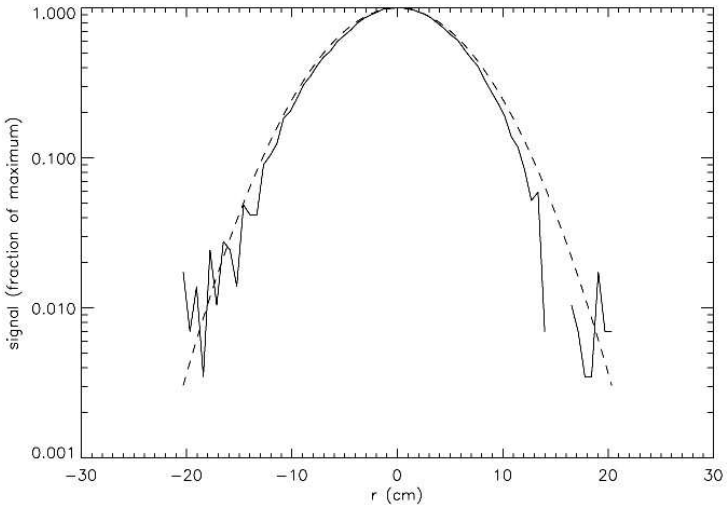

Fig. 4.4: A beam map from the 100 GHz horn #9.

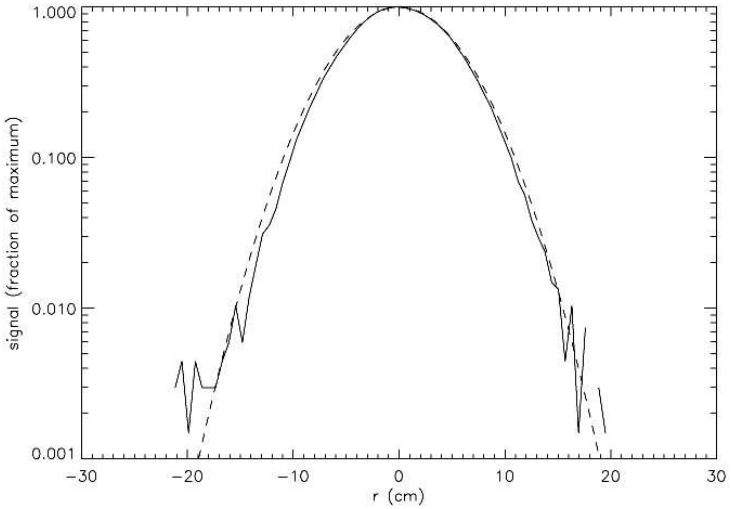

Fig. 4.5: A beam map from the 150 GHz horn #2.

$$P(r) \propto \int_{\text{aperture}} \frac{1}{\omega^2} \exp\Big(-\frac{2r^2}{\omega^2}\Big)\, dA \tag{4.6}$$

The finite aperture correction affects the beam size and shape much less than the polychromatic correction.

Thirdly, the vacuum inside the dewar curves the dewar window noticeably. The room temperature refractive index of the HDPE used for the window is $n = 1.52$ at microwave frequencies. The window's concavity slightly lenses the incoming radiation. However, a ray tracing simulation predicts at most a 0.2% effect on the beam width. Figures 4.4 and 4.5 do not incorporate any of the three previous effects.

Next, the beam axis may not be perfectly perpendicular to the bottom wall of the beam mapper. The measured beam patterns are slightly asymmetrical, suggesting that the horn may have been pointing slightly askew. This problem affects the beam shape only. The beam width goes as $\cos\alpha$, where α is the angle of the horn with respect to the normal to the bottom wall of the beam mapper. The effect is negligible because α is very small.

Finally, the filter cap is electrically conductive. Therefore, it acts as an electromagnetic waveguide, effectively extending the feed horn. This extension narrows the beam in its far field. Furthermore, the horn is designed to propagate single-moded radiation; the filter cap is not. Therefore, the filter cap affects the beam shape unpredictably. Although we have not modelled the beam defined by the horn and the filter cap, we expect the filter cap effect to be the dominant cause of the difference between the measured and expected beam patterns. The narrowing does not threaten QUaD's functionality, but an electrically non-conductive filter cap may correct the problem. The cap still must conduct heat well so that the band-defining filters cool to the same temperature as the rest of the focal plane.

5. OPPORTUNITIES FOR ADDITIONAL RESEARCH

This thesis has demonstrated that a QUaD pixel functions well at both 100 GHz and 150 GHz. It has also identified some opportunities for improving performance. The 100 GHz optical testing will continue into Summer 2004. The most important concern is to eliminate the out-of-band leak. Improved filtering will likely reduce the cross-polarization at 100 GHz from 7.5% to around 2%, a level comparable to that seen in the 150 GHz tests.

For the 150 GHz configuration, it may also be useful to measure the transmission function on the FTS again and to confirm the absence of out-of-band leaks with a thick grill filter. Repeating the tests would improve the confidence in the data taken with the PSB 150-02 module, in which the two PSBs are electrically shorted. The higher frequency noise in the 150 GHz transmission function may improve considerably with a better bolometer.

Understanding the spatial response at both frequencies would benefit from a thorough model of the horn with its filter cap. Additionally, an electrically insulating but thermally conductive filter cap would not alter the feed horn's beam definition. Building such a cap would be the best solution in the unlikely event that the narrowing effect of the metal filter cap degrades QUaD's performance.

Appendix A

SENSITIVITY CALCULATION

Experiments measuring the total power of the CMB generally define sensitivity in terms of the noise equivalent temperature (NET). The quotient of the NET and the square root of the observing time gives the smallest CMB temperature fluctuation to which the experiment is sensitive. In general, the noise equivalent power (NEP) is a measurable quantity from which the NET is derived. To convert from NEP to NET, first note that the optical power is proportional to the Planck brightness.

$$P \propto B_\nu \tag{A.1}$$

The Planck brightness is

$$\begin{aligned} B_\nu &= \frac{2h}{c^2}\frac{\nu^3}{e^x - 1} \\ x &\equiv \frac{h\nu}{k_{\rm B} T_{\rm CMB}} \end{aligned} \tag{A.2}$$

The derivative of eq. (A.1) is

$$\begin{aligned} \frac{dP}{P} &= \frac{dB_\nu}{B_\nu} \\ &= \frac{dB_\nu}{dT}\frac{dT}{B_\nu} \\ &= \frac{xe^x}{e^x - 1}\frac{dT}{T_{\rm CMB}} \end{aligned} \tag{A.3}$$

dP and dT represent the noise. For an NET relevant to the CMB,

$$\mathrm{NET} = \Big(\frac{e^x - 1}{xe^x}\Big)\Big(\frac{\mathrm{NEP}}{P_{\rm CMB}}\Big)T_{\rm CMB} \tag{A.4}$$

$$P_{\rm CMB} = \eta\varepsilon A\Omega B_\nu \Delta\nu \tag{A.5}$$

The Rayleigh-Jeans limit, such as in eq. (A.8), may not be used here.

Bowden et. al.[1] give the following derivation for the sensitivity of CMB polarization experiments.

A.1 Photon noise

Photon noise in a bolometer depends on the frequency ν, the bandwidth $\Delta\nu$, and the power P_ν in that bandwidth. The constant m is the number of polarization states detected. For a single PSB, $m = 1$.

$$\mathrm{NEP_{phot}}^2 = 2h\nu P_\nu + \frac{2P_\nu^2}{m\Delta\nu} \tag{A.6}$$

The power in the frequency band depends on the detector's optical efficiency η, the emissivity of the source ε, the optical throughput of the system $A\Omega$, the blackbody radiation intensity B_ν, and the bandwidth $\Delta\nu$.

$$P_\nu = \frac{1}{2}\eta\varepsilon A\Omega B_\nu \Delta\nu \tag{A.7}$$

The rejection of one linear polarization, or half of an unpolarized signal, introduces the factor of 1/2. For a diffraction-limited system such as QUaD, $A\Omega = \lambda^2 = (c/\nu)^2$. A rough derivation involves the Rayleigh criterion, $\sin\theta \approx \theta = \lambda/D$, where D is the diameter of the mirror. Because $D^2 \sim A$ and $\theta^2 \sim \Omega$, then $D^2\theta^2 = A\Omega = \lambda^2$. The proportionality constants cancel exactly in a rigorous derivation.

In the Rayleigh-Jeans limit,

$$P_\nu = \eta k_\mathrm{B} T_\mathrm{RJ} \Delta\nu \tag{A.8}$$

where T_RJ is the Rayleigh-Jeans temperature. The Rayleigh-Jeans temperature from QUaD's total optical loading, including the CMB, the atmosphere, the telescope, the dewar window, the lenses, and the filters, is expected to be $T_\mathrm{load} = 24.0$ K.[3]

A.2 Bolometer noise

The thermal conductance G—see eq. (B.5)—from the thermistor's electrical leads and the absorber supports to the 300 mK heat sink determine the extent of thermal fluctuations in the PSB. As in any bolometer, these fluctuations are the inherent bolometer noise, or phonon noise, and fundamentally limit its sensitivity.[6]

$$\mathrm{NEP_{bol}}^2 = 4k_\mathrm{B} T_\mathrm{bolo}^2 G \tag{A.9}$$

A.3 Amplifier noise

The electronics amplifiers also introduce noise into the system. It has been previously measured to be $\mathrm{NEP_{amp}} = 3.6 \times 10^{-17}$ W $\mathrm{Hz}^{-1/2}$.

All of the NEPs added in quadrature give $\mathrm{NEP_{tot}}$, from which the NET may be calculated.

$$\mathrm{NEP_{tot}} = \sqrt{\mathrm{NEP_{phot}^2} + \mathrm{NEP_{bol}^2} + \mathrm{NEP_{amp}^2}} \tag{A.10}$$

Appendix B

POLARIZATION-SENSITIVE MICROWAVE BOLOMETERS

Runyan[4] provides much of the following description of bolometers.

To a good approximation, a bolometer's resistance is

$$R_{\rm bolo}(T_{\rm bolo}) = R_0 e^{\sqrt{\frac{\Delta}{T_{\rm bolo}}}} \tag{B.1}$$

Both R_0 and Δ are constants specific to each thermistor. This relation is valid only when the electric field across the thermistor is below a certain threshold. Beyond that threshold, an electric field effect term with a different temperature dependence becomes significant. Equation (B.1) should be used only when $R_{\rm bolo}$ is low enough for the E-field term to contribute negligibly. The bolometer temperature in that regime is

$$T_{\rm bolo} = \frac{\Delta}{[\ln(R_{\rm bolo}/R_0)]^2} \tag{B.2}$$

Determining R_0 and Δ for a particular bolometer requires measuring its resistance at a range of temperatures. The measurement should take place in a cold, dark dewar so that no optical power loads the bolometer and changes its temperature. A heater controls the temperature $T_{\rm base}$ of the base on which the bolometer rests. A small voltage bias permits a measurement of the signal voltage and hence $R_{\rm bolo}$. The bias must be small enough that the electrical power dissipated in the bolometer does not heat it significantly above $T_{\rm base}$. A large voltage bias would heat the bolometer faster than the imperfect, finite thermal conductance between the bolometer and the base could sink the electrical heat. The set of measured $R_{\rm bolo}$ and $T_{\rm base}$ may be fit to eq. (B.1) to determine R_0 and Δ.

Thus, all the parameters of eq. (B.2) are measurable. Therefore, a measurement of V_s gives $T_{\rm bolo}$. $T_{\rm bolo}$ must be converted to optical power because measuring optical power is the purpose of the detector. The power balance equation relates the electrical power

$$\begin{aligned} P &= \frac{V_s^2}{R_{\text{bolo}}} \\ &= \frac{V_s(V_b - V_s)}{2R_L} \end{aligned} \tag{B.3}$$

dissipated in the bolometer and the optical power Q absorbed by the bolometer to T_{bolo}.

$$P + Q = \int_{T_{\text{base}}}^{T_{\text{bolo}}} G(T)\, dT \tag{B.4}$$

$G(T)$ is the bolometer's thermal conductance to the heat sink at temperature T_{base}. To a good approximation,

$$G(T) = G_0 \Big(\frac{T}{T_0}\Big)^{\beta} \tag{B.5}$$

G_0 is another constant specific to a particular bolometer. It is referenced to the redundant constant T_0 such that $G_0 = G(T_0)$. An empirical fit to the data determines G_0 and the exponent β.

Determining G_0 and β requires a full load curve, which is a set of signal voltage measurements at a range of bias voltages. The procedure is very similar to the one to measure R_0 and Δ. The two differences in this measurement are that the dewar need not be dark and the bias need not be small. In fact, a large range of bias voltages yields a more accurate fit as long as the bias does not exceed the threshold for the E-field effect to appear. From the measured V_s and the applied V_b, eq. (B.3) gives the electrical power P, and eq. (B.2) gives the bolometer temperature T_{bolo}. Evoking eq. (B.5), the expansion of the power balance equation (B.4) is

$$P + Q = \frac{G_0}{(\beta+1)T_0^{\beta}} \big(T_{\text{bolo}}^{\beta+1} - T_{\text{base}}^{\beta+1}\big) \tag{B.6}$$

The data may be fit to the derivative of eq. (B.6) with respect to T_{bolo}:

$$\frac{dP}{dT_{\text{bolo}}} = G_0 \Big(\frac{T_{\text{bolo}}}{T_0}\Big)^{\beta} \tag{B.7}$$

Q and T_{base} do not depend on T_{bolo}. Therefore, eq. (B.7) allows a fit to G_0 and β independent of the optical power and the base temperature.

The constants G_0 (and its T_0), β, R_0, and Δ are the four invariant parameters needed to deduce the absolute optical power incident on a bolometer. Equations (B.3) and (B.6) give

$$Q = \frac{G_0}{(\beta+1)T_0^{\beta}}\left(T_{\rm bolo}^{\beta+1} - T_{\rm base}^{\beta+1}\right) - \frac{V_s(V_b - V_s)}{2R_L} \tag{B.8}$$

where eq. (B.2) gives $T_{\rm bolo}$, which depends on R_0 and Δ. The experimenter determines the quantities $T_{\rm base}$, V_b, and R_L. V_s is the only measured quantity.

The uncertainty on the four bolometer parameters makes bolometers insensitive devices for measuring absolute optical power. However, they are highly sensitive for measuring differential optical power. Equation (B.8) may be expressed as

$$Q = g(T_{\rm bolo}) - P \tag{B.9}$$

The quantity $g(T_{\rm bolo})$ depends only on the bolometer temperature, or equivalently, the bolometer resistance through the relation in eq. (B.1). Therefore, $I_{\rm bias}$—and hence P—may be adjusted for any Q such that $T_{\rm bolo}$ remains constant. In that case,

$$\begin{aligned} Q_2 - Q_1 &= P_1 - P_2 \\ &= \frac{R_{\rm set}}{(R_{\rm set} + 2R_L)^2}(V_{b1}^2 - V_{b2}^2) \end{aligned} \tag{B.10}$$

where V_{bi} is the bias voltage that gives the constant $R_{\rm bolo} = R_{\rm set}$ when the bolometer looks at source i.

Appendix C

FOURIER TRANSFORM SPECTROSCOPY

Figure 2.5 displays a Fourier transform spectrometer (FTS). The device is essentially a Michelson interferometer. The movable mirror adjusts the only changing parameter: optical path length difference $x \equiv 2\Delta L$. At $x = 0$, the two beams recombine exactly in phase. As ΔL increases (or decreases), the radiation from the cold load, which contains the full blackbody spectrum, interferes destructively at some frequencies. A certain path length difference emphasizes some frequencies and de-emphasizes others. A graph of signal strength plotted versus ΔL is called an interferogram, and it is the inverse Fourier transform of the product of QUaD's spectral response function and the radiation reaching the dewar window.

Weisstein[7] gives a complete description of an FTS. The intensity $I_k(x)$ of radiation at a certain wave number k for a path length difference x is given by

$$I_k(x) = B(k)\langle T(k)\rangle \frac{1}{2}[1 + \cos(kx)] \tag{C.1}$$

$B(k)$ is the intensity of the incident radiation at a wave number k, and $\langle T(k)\rangle$ is the beamsplitter transmission function averaged over both polarizations. The intensity of radiation reaching the PSBs is $B(k)\langle T(k)\rangle J_Q(k)$ where $J_Q(k)$ is the transmission function of the QUaD test bed. The total radiation intensity at the PSBs is the integral over all k, or simply the inverse cosine Fourier transformation of $\langle T(k)\rangle B(k) J_Q(k)$:

$$\begin{aligned} I(x) &\equiv \int_0^\infty I_k(x)\, dk \\ &= \frac{1}{2} I(0) + \frac{1}{2}\mathfrak{F}_c^{-1}[\langle T(k)\rangle B(k) J_Q(k)] \end{aligned} \tag{C.2}$$

Taking a cosine Fourier transformation of both sides of the equation is needed to recover the incident radiation intensity. This Fourier transformation is defined to be $S(k)$.

$$\begin{aligned} \langle T(k)\rangle B(k) J_Q(k) &= 2\mathfrak{F}_c\Big[I(x) - \frac{1}{2}I(0)\Big] \\ &\equiv S(k) \end{aligned} \tag{C.3}$$

In practice, the interferogram cannot be extended to infinite ΔL. The truncation of the interferogram creates artificial sidelobes on the Fourier transformed spectrum. An apodization function $W(x)$, or a window over the interferogram, can reduce the sidelobes significantly. Therefore, the Fourier transformation of the interferogram multiplied by the apodization function is the convolution of $S(k)$ and the "instrument function" $w(k)$. The instrument function is the Fourier transform of the apodization function.

$$\begin{aligned} S_{\rm obs}(k) &= 2\mathfrak{F}_c\Big\{W(x)\Big[I(x) - \frac{1}{2}I(0)\Big]\Big\} \\ &= \mathfrak{F}_c[W(x)] \otimes \mathfrak{F}_c\Big[I(x) - \frac{1}{2}I(0)\Big] \\ &\equiv w(k) \otimes S(k) \end{aligned} \tag{C.4}$$

We use a Hanning apodization function, given by

$$W_{\rm Hanning}(x) = \cos^2\Big(\frac{\pi x}{2x_{\rm max}}\Big) \tag{C.5}$$

where $x_{\rm max}$ is the largest optical path length difference. Its instrument function is

$$w_{\rm Hanning}(k) = \frac{x_{\rm max}\ \mathrm{sinc}(2\pi k x_{\rm max})}{1 - 4x_{\rm max}^2 k^2} \tag{C.6}$$

where

$$\mathrm{sinc}\ x \equiv \frac{\sin x}{x} \tag{C.7}$$

Apodization slightly limits spectral resolution. The total translation of the movable mirror determines the resolution, but the half width at half maximum, η, of the apodization instrument function augments the resolution. For the Hanning function, $\eta = 2$.

$$\Delta\nu = \frac{\eta c}{4x_{\rm max}} \tag{C.8}$$

The largest frequency accessible $\nu_{\rm max}$ for a given optical path length difference step size Δx is

$$\nu_{\rm max} = \frac{c}{\Delta x} \tag{C.9}$$

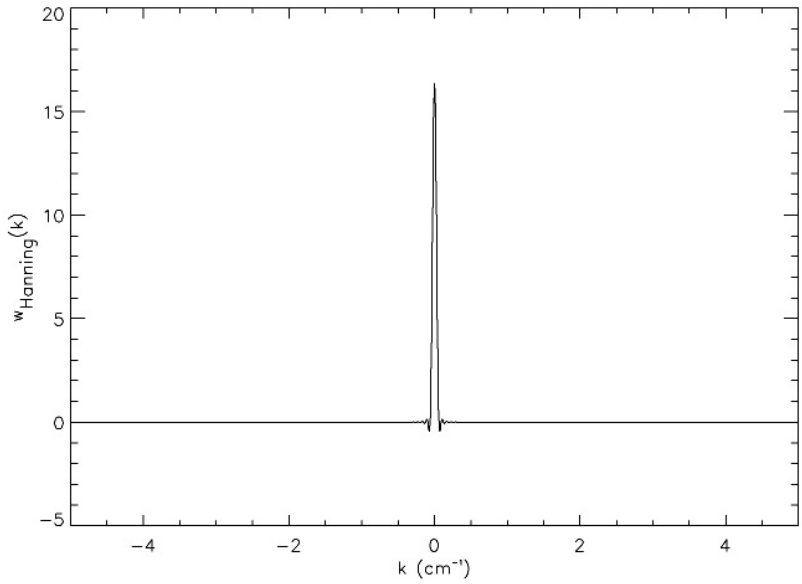

Fig. C.1: $w_{\mathrm{Hanning}}(k)$ for $x_{\max} = 16.36$ cm, such as for the 150 GHz interferogram in fig. 2.7.

The Hanning instrument function is approximately a delta function for large $x_{\max}$ (see fig. C.1). The convolution in eq. (C.4) disappears and $S_{\mathrm{obs}}(k) \approx S(k)$. Therefore, QUaD's transmission function is simply

$$J_Q(k) \cong \frac{S_{\mathrm{obs}}(k)}{\langle T(k) \rangle B(k)} \tag{C.10}$$

Because the dewar spends equal time looking at 77 K and 300 K blackbody spectra, $B(k)$ is the difference of the two.

$$\begin{aligned} B(k) &= B(k, T_2) - B(k, T_2) \\ &= 2hck^3 \Big(\frac{1}{e^{hck/k_{\mathrm{B}}T_2} - 1} - \frac{1}{e^{hck/k_{\mathrm{B}}T_1} - 1} \Big) \end{aligned} \tag{C.11}$$

77 K and 300 K blackbody spectra lie well within the Rayleigh-Jeans regime for QUaD's spectral bands.

$$B(k) = 2k^2 k_{\mathrm{B}} (T_2 - T_1) \tag{C.12}$$

The beamsplitter transmits the two different polarizations of incoming radiation differently. The most convenient polarization basis is the one formed by the vectors parallel and perpendicular to the plane of the beamsplitter. The transmission function for a given polarization T_p is the square of the ratio of the transmitted electric field to the incoming electric field.

$$T_p \equiv \left|\frac{E}{E_0}\right|^2 = \frac{16R_p(1-R_p)^2\sin^2(\frac{1}{2}\delta)}{[(1-R_p)^2+4R_p\sin^2(\frac{1}{2}\delta)]} \tag{C.13}$$

R_p is the Fresnel reflection coefficient for the polarization p. The variable δ depends on the beamsplitter thickness d, the index of refraction of the beamsplitter material n, the index of refraction of the spectrometer medium (air) n_0, the wavelength of the radiation in vacuum λ_0, and the angle of the beamsplitter with respect to the incoming radiation θ.

$$\delta \equiv \frac{4\pi d}{\lambda_0}\sqrt{\left(\frac{n}{n_0}\right)^2 - \sin^2\theta} \tag{C.14}$$

The Fresnel reflection coefficients depend on θ and the dielectric constant of the beamsplitter material ϵ.

$$R_\parallel = \left(\frac{\epsilon\ \cos\theta - \sqrt{\epsilon - \sin^2\theta}}{\epsilon\ \cos\theta + \sqrt{\epsilon - \sin^2\theta}}\right)^2 \tag{C.15}$$

$$R_\perp = \left(\frac{\cos\theta - \sqrt{\epsilon - \sin^2\theta}}{\cos\theta + \sqrt{\epsilon - \sin^2\theta}}\right)^2 \tag{C.16}$$

The index of refraction depends on the dielectric constant ϵ and the relative permeability μ, where $\mu \approx 1$ for most common materials.

$$n = \sqrt{\epsilon\mu} \approx \sqrt{\epsilon} \tag{C.17}$$

The average of the transmission function over polarizations is an arithmetic average.

$$\langle T(k)\rangle = \frac{T_\parallel + T_\perp}{2} \tag{C.18}$$

The beamsplitting material for the QUaD FTS is mylar, which has an index of refraction $n \approx 1.74$. The index of refraction of air is $n_0 = 1$. (The effect of the tiny deviation from 1 is entirely negligible.) Incoming radiation strikes the beamsplitter at $\theta = 45°$, as shown in fig. 2.5.

BIBLIOGRAPHY

[1] M. Bowden *et al.*, Mon. Not. Roy. Astron. Soc. **349**, 321 (2004), astro-ph/0309610.

[2] W. C. Jones, R. S. Bhatia, J. J. Bock, and A. E. Lange, (2002), astro-ph/0209132.

[3] S. Church *et al.*, New Astron. Rev. **47**, 1083 (2003).

[4] M. C. Runyan, PhD thesis, California Institute of Technology, 2002.

[5] J. Lesurf, *Millimetre-wave Optics, Devices, & Systems* (Adam Hilger, Bristol, UK, 1990).

[6] J. J. Bock, D. Chen, P. Mauskopf, and A. E. Lange, Space Science Rev. **74**, 229 (1995).

[7] E. W. Weisstein, PhD thesis, California Institute of Technology, 1996.